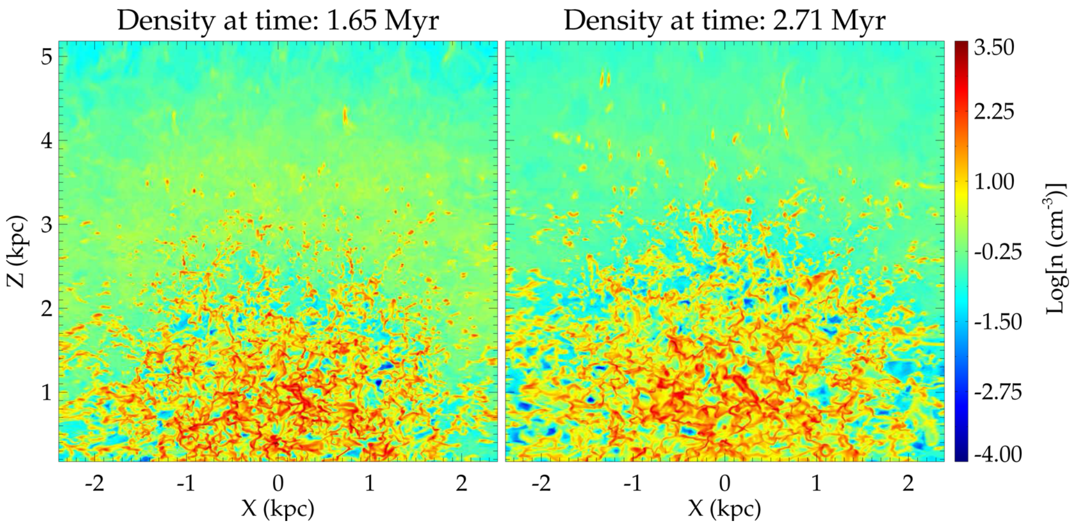

Figure 1. Density ($\log[n(\mathrm{cm}^{-3})]$) in the x–z plane for settling turbulent ISM at two different times. The ISM develops a filamentary structure, typical of a turbulent medium.

Dopita 1993; Allen et al. 2008). Cooling down to 10^6 K proceeds with equilibrium ionization and cooling, until the cooling becomes rapid compared to the recombination time-scales and the ionization lags behind, being more ionized at a given temperature than in equilibrium. Below 10^6 K, the cooling rates increase to a maximum around $\sim 10^5$ K, before falling rapidly below 10^4 K. At each point, the full ionization state including electron densities and atomic level populations, are solved, allowing the cooling and a simple equation of state to be inferred from the self-consistently changing mean molecular weight $\mu(T)$. The gas is assumed to be atomic, and to have an ideal adiabatic index of 5/3. The temperature-dependent cooling function and mean molecular weight thus obtained were tabulated as a function of the ratio of pressure and density (p/ρ), which are PLUTO primitive variables. The cooling losses ($[\rho/\mu(T)]^2\Lambda(T)$) for each cell in the PLUTO domain were applied by interpolating the cooling function and mean molecular weight from the tabulated list.

3 SETTLING OF ISM

(i) Filamentary ISM: we initialize the velocity in the warm cloudy medium with a turbulent velocity distribution, modelled as a random Gaussian variate for the three velocity components with a Kolmogorov spectrum in Fourier space. We set the velocity dispersion of the clouds higher than that of the baryonic dispersion of the galaxy and let the clouds settle in the potential. The fractal clouds disperse and shear due to the turbulent motions and cloud–cloud collisions. The clouds eventually condense into filaments, typical of a turbulent medium (e.g. Federrath & Banerjee 2015; Federrath 2016) as shown in Fig. 1. After $\sim$1 Myr, the turbulent distribution settles into a two phase medium (see Fig. 1) characterized by a distribution of warm filaments extending up to $\sim$2 kpc and an HH extending to larger radii.

(ii) Density PDF and two phase ISM: in Fig. 2, we show the volume-weighted probability distribution function (PDF)[2] of the density at different times of the simulation. Initially ($t = 0$), the

[2] The volume-weighted PDF of variable is constructed by evaluating the histogram and counting the fractional volume of a simulation cell as the weights for a histogram bin.

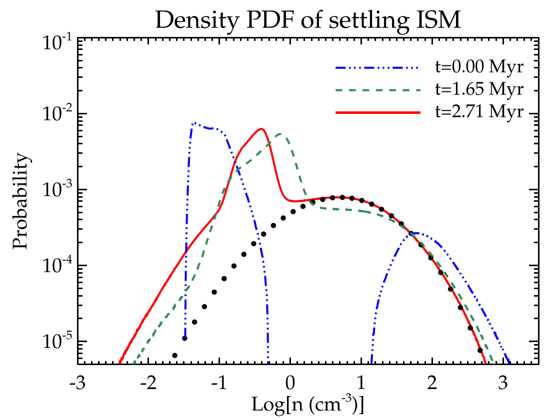

Figure 2. The PDF of the density ($\log[n(\mathrm{cm}^{-3})]$) for a settling ISM without jet, at $t = 0$ (dash–dotted in blue), $t = 1.65$ Myr (dashed in green) and $t = 2.66$ Myr (solid red). The black dotted lines represent a fit to the high-density end of the PDF following equation (A7).

density PDF shows two distinct distributions: (a) the warm fractal clouds with high density, (b) a low-density HH. As the ISM evolves under the influence of the turbulent velocity field and gravity, the density PDF changes due to shearing of the clouds. The density PDF converges well after 1 Myr into a two component PDF corresponding to a two phase medium. The turbulent motions result in stripping of the dense clouds, lowering the mean of the high-density component of the PDF. The dispersed cloud mass forms a denser halo of gas near the central region.

Density structures formed as a result of hierarchical turbulent processes are expected to exhibit a lognormal probability distribution (e.g. Vazquez-Semadeni 1994; Padoan, Jones & Nordlund 1997; Klessen 2000). However, recent simulations have shown significant deviation from a lognormal behaviour in the tail of the distribution (Federrath et al. 2010; Konstandin et al. 2012; Federrath & Klessen 2013; Federrath & Banerjee 2015). Hopkins (2013) has shown that a lognormal-like distribution modified by the influence of intermittency from turbulent shocks is a better descriptor of the PDF in such cases (see Appendix A for a brief summary of the analytical expressions). For our simulations, we find the Hopkins

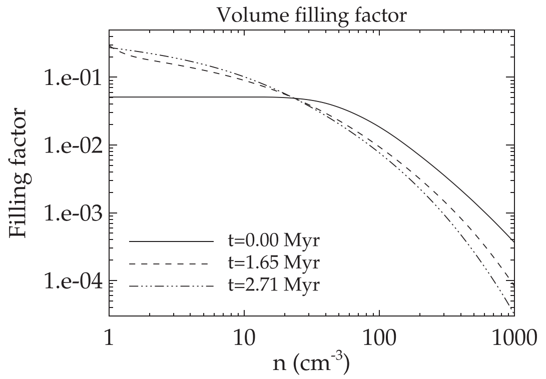

Figure 3. The volume filling factor as a function of density (in cm^{-3}) for a settling ISM.

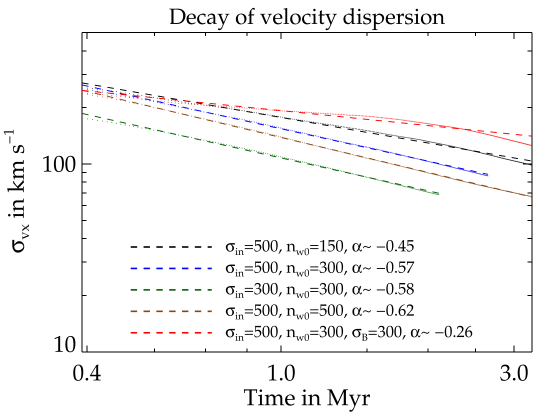

Figure 4. Comparison of the dispersion of V_x (in kms^{-1}) for different simulations. $\sigma_{\rm in}$ (in kms^{-1}) is the initial velocity dispersion, $n_{\rm w0}$ (in cm^{-3}) the mean central density of the warm phase, $\sigma_{\rm B}$ (in kms^{-1}) is the dispersion of the baryonic component of the gravitational potential and α is the exponent for a power-law fit to the profiles ($\sigma_{vx} \propto t^{\alpha}$).

function to provide a good fit to the high-density component of the PDFs. For example, the black-dotted line in Fig. 2 shows the Hopkins function with parameters $\bar{\rho} = 15$ cm^{-3}, $\sigma_{\rho} = 39.78$cm^{-3}, $\eta = 0.08$, which provides a good fit to the high-density portion of the PDF at $t \sim 2.7$ Myr. For the rest of the paper, we have used the Hopkins function to fit the high-density end of the density PDF and compare the statistics of the ISM under different conditions.

(iii) Volume filling factor: in Fig. 3, we show the change in the volume filling factor, defined as the total volume occupied by the gas beyond a threshold density, plotted as a function of density. At $t = 0$, the volume filling factor for $n > 10$ is $\lesssim$0.045. As the clouds shear and settle into filaments, the filling factor is lowered for the high-density cores as the some of the warm gas is dispersed.

(iv) Decay of turbulence: as the clouds settle, the velocity dispersion decreases as a power law with time. A power-law decay of velocity dispersion (with exponent ~1.2–2) is typical of hydrodynamic supersonic turbulence (Mac Low et al. 1998; Stone, Ostriker & Gammie 1998). The rate of decay does not depend on the initial velocity dispersion. For example, as shown in Fig. 4, the rate of decay for $\sigma_{\rm in} = 500$ and $\sigma_{\rm in} = 300$ for the same $n_{\rm w} = 300$ is similar (with the power-law exponent $\alpha \sim -0.58$. However, as a result of the presence of atomic cooling and external gravity, the rate of settling depends on the mean cloud density and the potential of the galaxy. The settling rate is slower for lower mean cloud density and a gravitational potential with higher stellar dispersion.

Table 3. Coefficients of the fit to the density PDF in Fig. 7 following equation (A7).

$Z_{\rm jethead}$ (in kpc)	$\bar{\rho}$ (in cm^{-3})^a	σ_{ρ} (in cm^{-3})^b	η	$\tilde{\rho}_{>10}$ (in cm^{-3})^c
0	21.38	52.68	0.14	50
1	18.42	44.17	0.14	43.96
3	15.73	27.9	0.12	33.56
5	13.21	20.52	0.17	29.5

Notes. ^{a}Mean density for the PDF.
^{b}Standard deviation of variable ρ, which is related to the standard deviation in $s = \ln \rho$ as in equation (A8).
^{c}Volume-weighted mean of density for $n > 10$ cm^{-3}. This gives a measure of the mean density of the high-density filaments.

4 JET SIMULATIONS

4.1 Evolution of the density of the ISM

We first let the ISM settle into a turbulent filamentary structure with a velocity dispersion ~100–150 km s^{-1}, which is typical of high-redshift galaxies (Förster Schreiber et al. 2009; Wisnioski et al. 2015). We then inject the relativistic jet whose parameters are described in Section 2.3. We list the simulations performed with jets interacting with the turbulent ISM in Table 2. In Figs 5 and 6, we present the evolution of the density, radial velocity, pressure and temperature of the ISM for simulation A. The jet is initially impeded by the dense filaments (Fig. 5) and passes through a flood-channel phase as described in previous works (Sutherland & Bicknell 2007; WB11; WBU12), seeking the paths of least resistance as it drives an energy bubble through the ISM.

The jet shears the dense filaments as it clears its path. The effect of shearing of the dense cores is well demonstrated through the evolution of the density PDF shown in Fig. 7. The high-density tail of the PDF is significantly reduced as the jet-driven bubble shears the clouds. There is a subsequent enhancement of the PDF at $n \sim$ 10–100 cm^{-3}, which occurs both as a result of compression of low-density gas from the forward shock and also of fragmentation of the dense filaments. Coefficients of fits (following equation A7) to the high-density end of the PDF are listed in Table 3. The density PDF converges after the jet breaks out (jet head $\gtrsim$3 kpc) and decouples from the ISM, proceeding along the cleared path.

The duration of the flood-channel phase of the jet evolution depends upon the mean density and filling factor of the ISM, as previously discussed in WBU12. Clouds with denser cores are less ablated and more efficiently impede the progress of the jet. In Fig. 8, we present the density for simulation B (Table 2), where a jet of power 10^{45} ergs^{-1} passes through a medium with lower mean density ($n_{\rm w0} = 150$ cm^{-3}) compared to that of simulation A. We note that the jet breaks out of the warm dense gas much faster, in comparison to simulation A.

4.2 Evolution of the energy bubble

The confined jet creates an expanding energy bubble. A fast moving forward shock first sweeps through the filaments heating the gas to ~10^5 K (see Fig. 6). The forward shock is followed by a slower moving region of nearly homogeneous high pressure, defining the energy bubble (see Fig. 6). The energy bubble shears the dense filaments as it expands into the ISM, accelerating the dense clouds to radial velocities in excess of ~300 kms^{-1} (as shown in Fig. 9), as also reported earlier in WBU12. Some of the clouds are dragged